ORIGINAL RESEARCH

Determination of the critical value of damage in a channel-die rotational compression test

Z. Pater[1] · J. Tomczak[1] · T. Bulzak[1] · Ł. Wójcik[1] · P. Walczuk[1]

Abstract

This article describes the problems involved in modelling material cracking in skew rolling processes. The use of the popular damage criteria is impossible because of the lack of a calibration test that would make it possible to determine the critical value of material damage under conditions similar to those found in skew rolling. To fill this gap, a test called channel-die rotational compression was proposed. It consisted of rolling a disk-shaped specimen in a cavity created by two channels of cooperating tools (flat dies), which had heights smaller than the diameter of the specimen. When the rolling path was sufficiently long, a crack formed in the axial zone of the specimen. In this test, modelling using the finite element method made it possible to determine the critical values of material damage. As an illustration, the test was used to determine the critical damage value when conducting a rotational compression process on 50HS steel (1.5026) specimens formed in the temperature range of 950–1200 °C. The analysis was conducted using the Cockcroft–Latham damage criterion.

Keywords Damage · Rotational compression · FEM · Experiment

Introduction

Material cracking is a frequent occurrence in skew rolling. In some processes of this type, such as the Mannesmann piercing process, cracking is desirable. In others, it is unacceptable because it induces irreparable damage to the product being formed. Therefore, it is important to monitor cracking beginning at the design stage of a given manufacturing process. High hopes are being pinned on the possibilities offered by computer modelling, which is increasingly used in the analysis of skew rolling processes.

The first reports on the modelling of the Mannesmann effect, which leads to the formation of a crack in the axial zone of a rolled product, were published at the beginning of the twenty-first century. Ceretti et al. [1] used Deform 2D software to model cracking (under the plane-strain assumption) in the axial zone of a part skew-rolled between flat tools. In their analysis, they adopted the theory of the maximum principal stress σ_1, assuming that the critical value of this stress was

30 MPa. When the principal stress in a given element was $\sigma_1 > 30$ MPa, the element was deleted to model crack formation. This model of cracking was used by Capoferri et al. [2] in their analysis of the formation of AISI1020 steel pipes (in this case, the limit value of principal stress σ_1 was assumed to be 36.5 MPa).

The first attempt to model the Mannesmann piercing process under 3D deformation was made by Ceretti et al. [3]. Their analysis was carried out using the Deform 3D software and introducing several simplifications such as ignoring the piercing plug and thermal phenomena that occur in a workpiece. The calculations were used to analyse the stress state of a product rolled with two rollers. A full 3D model of the rotary piercing process, which took into account the thermal behaviour of the material during forming, was developed by Pater et al. [4]; however, this model was not used to analyse material cracking. A breakthrough study in this area was conducted by Fanini et al. [5]. In their study, the Forge software and Lemaitre damage law were used to model the cracking in the axial zone of a cylindrical billet. This included the requirement of introducing the initial distribution of the damage in the billet into the model, which was a consequence of the continuous casting process used to form the billet. The modelling results were in good agreement with the experimental results. This method of modelling crack formation was later

✉ Z. Pater
  z.pater@pollub.pl

[1] Lublin University of Technology, 36 Nadbystrzycka Str, 20-618 Lublin, Poland

used in the analyses carried out by Chastel et al. [6] and Ghiotti et al. [7]. Other damage criteria have also been used in the analysis of the piercing process. For example, Pater and Tofil [8] used the Cockcroft–Latham criterion to identify the regions that were most susceptible to cracking. Using the same criterion, Skripalenko et al. [9] determined the effect of rollers on the plasticity of billets. The material cracking was not modelled in either study because the critical damage value was unknown.

It is also necessary to model the effective separation (or failure) of the material in the analysis of helical-groove rolling processes, in which parts rolled in roll passes (formed by the helically cut grooves of two cooperating rollers) are cut off from the billet [10]. Earlier versions of specialised software did not make it possible to model the material separation, which is why it was a common practice in simulation studies to leave small connectors (bridges) between workpieces such as balls or stepped shafts [11–14]. Recently, however, theoretical models of rolling processes for the production of balls [15, 16] and ball pins [17] have been developed in which the separation of the material has effectively been simulated. In these models, the Cockcroft –Latham damage criterion was used, with the critical damage value arbitrarily chosen to be in the range of 2–3. It should be emphasised that this value range was selected intuitively and was not based on scientific data. Therefore, we found it necessary to develop a test to determine the critical damage value, which could be applied to skew rolling processes. This type of test, which is called channel-die rotational compression, was developed at the Lublin University of Technology and was the focus of this study. The test is discussed using the example of forming 50HS steel (1.5026) specimens, which can be used in processes such as the helical rolling of grinding mill balls.

Concept of rotational compression between channel-dies

A schematic of the channel-die rotational compression test is shown in Fig. 1, which features selected parameters of the process. In this test, a cylindrical specimen with diameter d_0 and width b is placed in a channel hollowed out in a fixed flat tool cooperating with a moveable tool with an identical channel. The distance between the channel
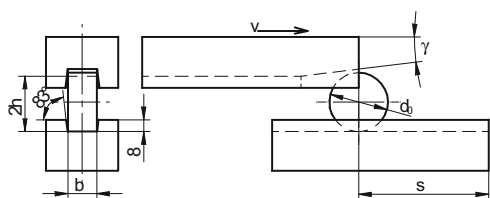

Fig. 1 Schematic of the test of rotational compression between channel-dies

bottoms (cavity height) is 2 h and is smaller than specimen diameter d_0. At the inlet to the channel of the moveable tool, a tapered cut is made at angle γ, which makes it possible to insert the specimen into the cavity (angle γ must be smaller than friction angle ρ; where ρ equals the tangent of the static friction coefficient for the material–tool friction couple). When the moving tool is set into motion, the specimen is compressed in a radial direction (perpendicular to the bottoms of the channels) and simultaneously rotated by frictional forces. This method of loading the specimen gives rise to a state of stress in its axial zone, which leads to the formation of a crack (the Mannesmann effect) when the forming path along which the specimen is compressed is long enough.

To determine the critical damage value, it is first necessary to experimentally establish the forming length s at which cracking occurs. Next, the test must be simulated using numerical modelling methods to determine the value of the damage function in the axial zone at the moment of crack formation. This value will be equal to the critical damage value sought.

Experimental tests of rotational compression between channel-dies

Experimental tests were carried out using a wedge rolling mill installed at the Lublin University of Technology. This mill has a hydraulic drive and makes it possible to form workpieces using flat tools with a maximum length of 1000 mm. The speed of the (upper) moveable tool is 300 mm/s. A general view of the rolling mill and its workspace adapted for use in the channel-die rotational compression test is shown in Fig. 2.

The test material was 50HS steel (1.5026), from which specimens with a diameter $d_0 = \emptyset 40$ mm and width $b = 20$ mm were formed. Before forming, the specimens were heated to temperature T (950 °C, 1000 °C, 1050 °C, 1100 °C, 1150 °C, or 1200 °C) in an electric chamber furnace. The specimens were then placed in the channel of the lower tool and compressed while being rotated over forming length s, assuming that the distance between the bottoms of the channels (height of the cavity) was 2 $h = 38$ mm. Figure 3 shows the characteristic stages of the test. By conducting tests with increasingly greater values for distance s, we determined the critical value of forming length above which cracking occurred. The critical forming length was assumed to be the maximum value for distance s (at a given temperature) for which no cracking of the material was observed in three repetitions of the test.

The samples deformed in the rotational compression test had dents on their front surfaces (side surfaces). The depths of

Fig. 2 Laboratory rolling mill used in the tests (top) and a view of workspace adapted for use in the test of rotational compression between channel-dies (bottom)

these dents increased with s. As a consequence of this deformation, the thickness of the axial zone of the specimens decreased, which resulted in the formation of a crack along the specimen's axis, running along the entire length of the specimen. A similar phenomenon was observed by Tomczak et al. [16] in helical ball-rolling processes when the roll pass was overfilled. In our case, the fact that cracking could be observed on the end faces of specimens facilitated the experiments. In addition, it was found that at lower forming temperatures, the crack grew rapidly after initiation, as shown in Fig. 4. In contrast, at high forming temperatures, crack propagation was much slower. First, numerous macrocracks appear, which then merge into one axial crack (Fig. 5).

During the experimental tests, the forming load (force needed to move the movable tool) was also measured. Figure 6 shows the forming load distributions obtained in tests in which specimens were compression-rolled over the critical forming length at six different temperatures. The force curves were used to validate the Forge finite element method (FEM) model of the rotational compression test. Based on an analysis of the obtained force values, it should be mentioned that the maximum values were reached in the initial phase of the process, when the sample was subjected to ovalisation. In a later formation phase, these values were slightly smaller, which was most likely caused by the change in the shape of the sample
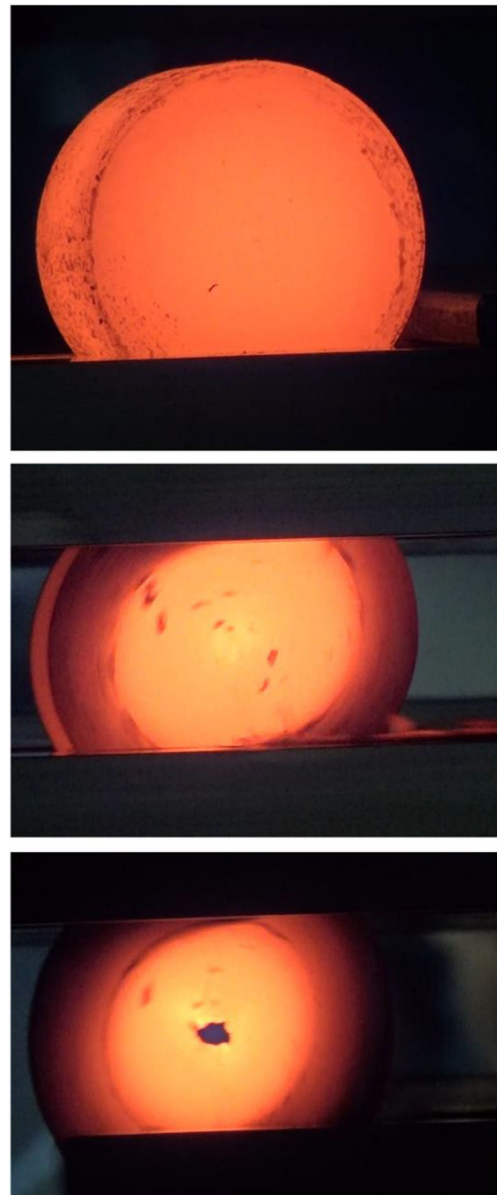

Fig. 3 Stages of compression of a billet preheated to 1000 °C rotated over distance $s = 250$ mm: (from top to bottom) positioning of the specimen in the channel, rotational compression, and crack formation

(the occurrence of front dents of increasing depth). At the end of the test, the forces decreased to zero as a result of the sample exiting the channel where the compression occurred.

Fig. 4 Deformed specimens obtained from billets (preheated to 950 °C) at forming lengths (s) of (from left to right) 150 mm, 175 mm, 200 mm, and 250 mm

Fig. 5 Deformed specimens obtained from billets (preheated to 1200 °C) at forming lengths (s) of (from left to right) 375 mm, 400 mm, 455 mm, and 500 mm

FEM analysis of rotational compression between channel-dies

A numerical model of the rotational compression between channel-dies was generated using the commercial simulation software package Forge® NxT v1.1. The geometric model of rotational compression is shown in Fig. 7 faithfully reproduces the test parameters used in the experiments. The specimen was modelled using mixed velocity-pressure linear tetrahedral elements. In order to enhance the accuracy of the calculations, the mesh size was assumed to be dependent on the workpiece radius R and equal to 0.25 mm for $R = 0–2.5$ mm, 0.5 mm for $R = 2.5–5$ mm, 1 mm for $R = 5–10$ mm, and 2 mm for $R > 10$ mm.

In the simulations, it was assumed that the material model of the tested 50HS steel (1.5026) was defined by the Hensel–Spittel equation:

$$\sigma_F = 1884.02 e^{-0.00288\,T}\,\varepsilon^{-0.2622}\,e^{-0.08651/\varepsilon}\,\dot{\varepsilon}^{0.13082}, \qquad (1)$$

where σ_F is the flow stress (MPa), ε is the effective strain (−), T is the temperature (°C), and $\dot{\varepsilon}$ is the strain rate (s^{-1}).

The presented 50HS grade steel model was taken from the data library of the Forge® software used in the research.

Friction was modelled using the Tresca model, assuming that the friction factor at the material/tool interface was 0.8
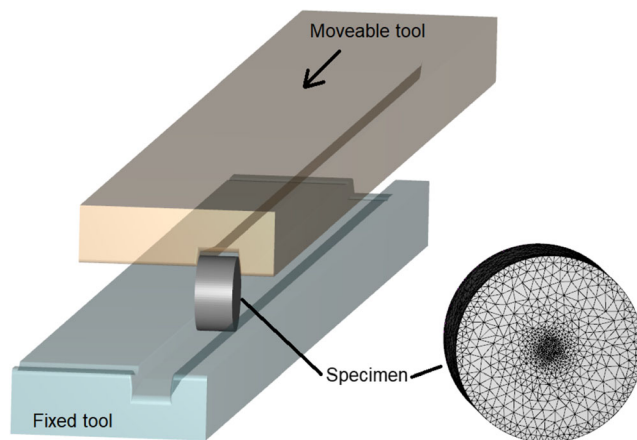
Fig. 7 Forge model of rotational compression showing workpiece (specimen) meshed with tetrahedral elements

[18]. In addition, it was assumed that during the compression the tools had a constant temperature of 50 °C and the coefficient of heat transfer between the specimen and tools was 10,000 W/m²K.

A total of six forming process cases were modelled at initial specimen temperatures of 950 °C, 1000 °C, 1050 °C, 1100 °C, 1150 °C, and 1200 °C, with respective critical forming lengths s corresponding to each of these temperatures. The course of one of these compression tests is presented in Fig. 8. An analysis of the data given in this figure shows that after being caught by the moving tool, the specimen was given a rotational motion, and its transverse outline was ovalised. An oval cross-sectional shape is typically obtained in skew rolling processes and maintained until the end of the forming process (Fig. 9), which is undoubtedly the result of the side walls of the channels counteracting the elongation of the specimen in the axial direction. This causes a stress state, conducive to the Mannesmann effect, to be generated in the specimen's axial zone along the entire forming length s.

To measure the stress state, three virtual sensors (labelled 1, 2, and 3) were placed along the specimen's axis (sensor 1 was located on the lateral surface, sensor 2 was placed 5 mm away from the lateral surface, and sensor 3 was 10 mm away from that surface, which means that it was located precisely in the centre of the specimen). The sensors registered the distributions of stress state components σ_x (Fig. 10), σ_y (Fig. 11), σ_z (Fig. 12), and τ_{yz} (Fig. 13); the distributions of tangential stresses τ_{xy} and τ_{xz} are not shown, because they proved to be insignificant (stresses ranged from −1 MPa to +1 MPa). An analysis of the data given in these figures showed that in the centre of the specimen, normal stresses acting in the x (axial) direction and y direction (the direction of motion of the moveable tool) had positive values (they were tensile stresses), whereas normal stresses acting in the z (vertical) direction had negative values (they were compressive stresses). In addition, intensive shear stresses occurred along the entire length of the specimen's axis in the yz plane (perpendicular to the
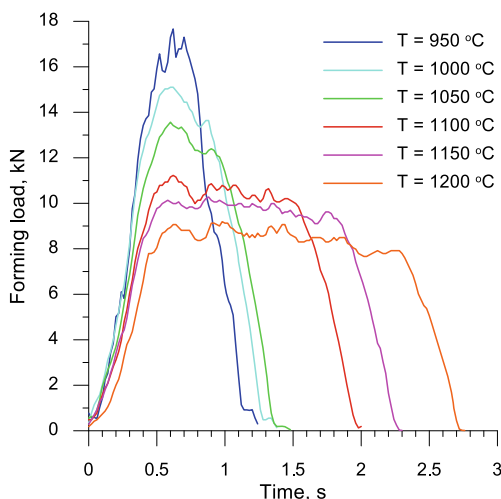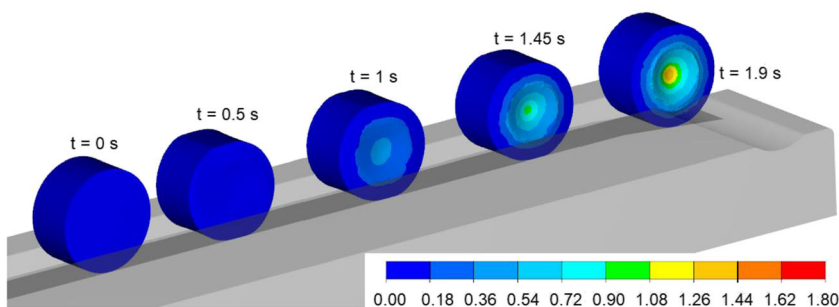

Fig. 6 Distributions of forming loads experimentally determined in tests of rotational compression between channel-dies, as function of billet temperature T

0.00 0.18 0.36 0.54 0.72 0.90 1.08 1.26 1.44 1.62 1.80

axis of specimen rotation). As a result of the rotation of the specimen (in the radial direction), stresses changed cyclically from compression to tensile and back again (there were 2 cycles of stress changes per revolution). As an effect of this state of stress, a crack formed after the specimen had made a critical number of revolutions.

An important parameter taken into account in the analysis of material cracking is the stress triaxiality [19], which is given by the following equation:

$$\eta = \frac{\sigma_m}{\sigma_i}, \qquad (2)$$

where η is the stress triaxiality (–), σ_m is the mean stress (MPa), and σ_i is the effective stress (MPa). In the late 1960s, McClintock [20] and Rice and Tracey [21] noticed that an increase in this parameter accelerated material cracking. Given this, we plotted the distribution curves of the stress triaxiality for three selected virtual sensors, as shown in Fig. 14. Based on the obtained charts it can be stated that after subjecting the sample to ovalisation, the values of stress triaxiality in the centre of the sample (sensors 2 and 3) were similar to those occurring during uniaxial tension, for which $\eta = 0.33$. However, on the front surface, the value of this parameter oscillated in the range of −0.1 to +0.1. It seemed that the lack

of stability for the value of stress triaxiality at sensor 1 could be explained by the constant changes in the shape of the front surface, where dents of increasing depth occurred along with an increase in the forming path.

Figure 15 shows the distribution of effective strain in a specimen preheated to 1100 °C and subjected to rotational compression over a distance $s = 275$ mm. It can be seen that the largest strain occurred on the lateral surfaces of the specimen at sites where the material rubbed against the side walls of the channel. Elevated strain was also found in the axial zone where cracking occurred. Undoubtedly, the strain was due to the intensive flow of the material on the surface perpendicular to the axis of the sample rotation.

Interesting information is provided by an analysis of the temperature distribution in a specimen subjected to rotational compression (Fig. 16). As a result of the material coming into contact with the tools, substantial cooling of the material is observed on the specimen's circumference. The temperature in these regions may drop by as much as 300 °C. Meanwhile, in the axial zone where the material fractures, the temperature remains at the same level as the initial temperature of the billet. Similar temperature changes are also visible in Fig. 3, which presents the stages of one of the laboratory tests.
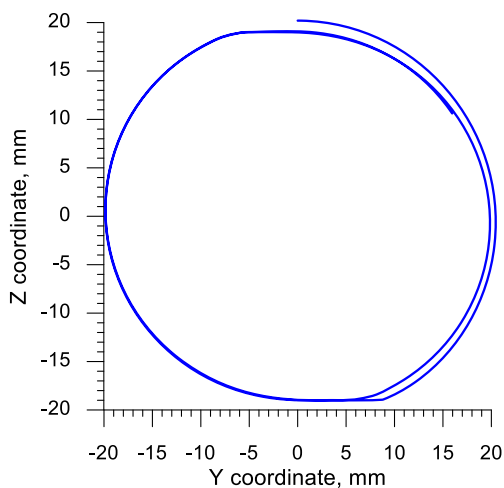

Fig. 9 Trajectory of point located on the outer surface of the specimen, on its rotation axis, for compression test of a billet preheated to $T = 1100$ °C
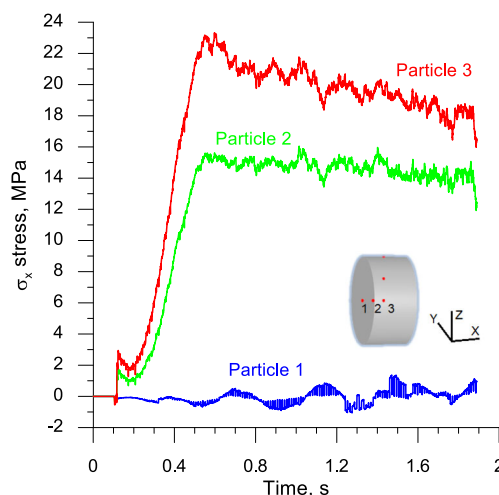

Fig. 10 Distribution of normal stress acting in the x direction (axial direction) at points 1, 2, and 3 located on the specimen's axis, with $T = 1000$ °C
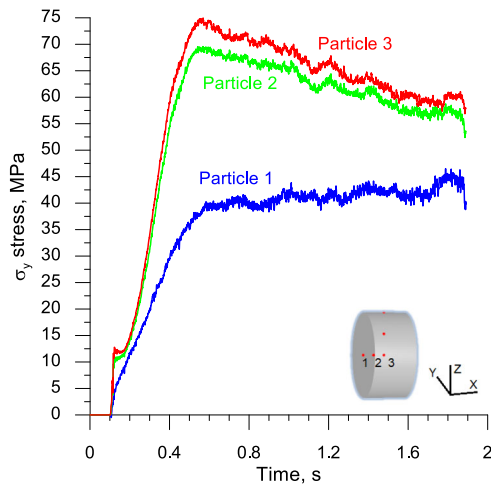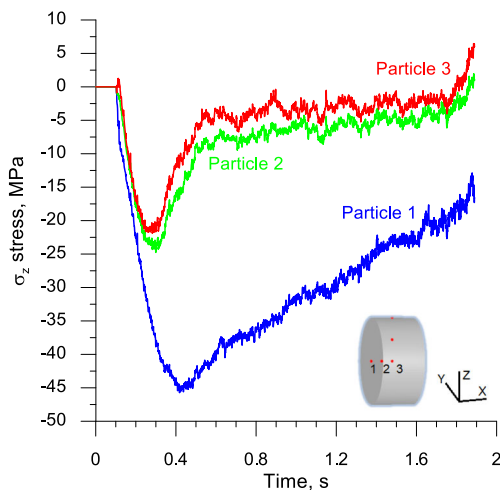
Fig. 11 Distribution of normal stress acting in the y direction (direction of movement of moveable tool) at points 1, 2, and 3 located on the specimen's axis, with T = 1000 °C
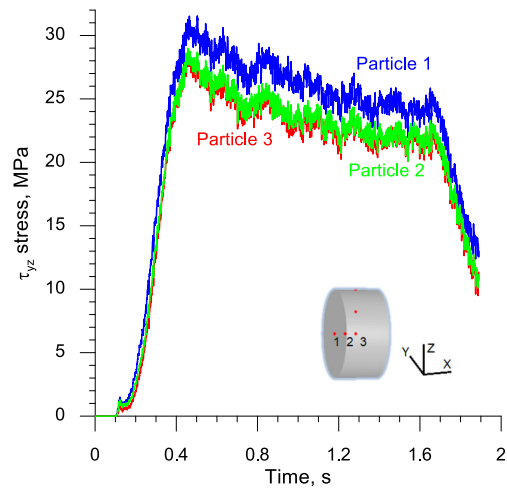

Fig. 13 Distribution of tangential stress acting in the yz plane (vertical plane perpendicular to the axis of specimen rotation) at points 1, 2, and 3 on the specimen's axis, with T = 1000 °C

The material cracking analysis was performed using the Cockcroft –Latham criterion [22], which is based on the calculation of the following damage function.

$$f_{CL} = \int_0^\varepsilon \frac{\langle \sigma_1 \rangle}{\sigma_i} d\varepsilon, \qquad (3)$$

where f_{CL} is the Cockcroft –Latham (CL) damage function (−), σ_1 is the maximum principal stress (MPa), σ_i is the effective stress (MPa), ε is the effective strain (−), and $\langle \rangle$ is a Macaulay bracket. The material starts to crack when function f_{CL} reaches its critical value (C_{CL}) as determined in calibration tests. Accurate cracking prediction results are obtained only when the stress state of the process under analysis is similar to that found in the calibration test [23].

The distribution of the damage function presented in Fig. 17, calculated in accordance with the CL criterion, shows

that the function takes maximum values in the axial zone, where cracking occurs. This confirms the possibility of applying this criterion to the modelling of skew rolling processes. To definitively determine whether rolling will lead to cracking, it is necessary to know the critical value of the damage function, C_{CL}.

Figure 18 shows the distributions of the forming loads in all six numerically analysed compression tests. A comparison of the calculated and measured loads (Fig. 6) shows that the computational and experimental results are in very good agreement in terms of quality. Quantitatively, the measured loads are approx. 1–1.5 kN higher than the calculated loads, which can be explained by additional friction (against the guides), which was not taken into account in the numerical analysis. For this reason, it was concluded that the comparison of the distributions of calculated and measured loads indicated
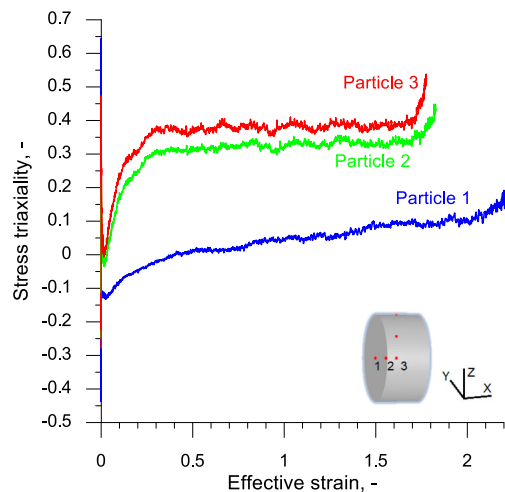

Fig. 12 Distribution of normal stress acting in the z direction (radial direction) at points 1, 2, and 3 located on the specimen's axis, with T = 1000 °C

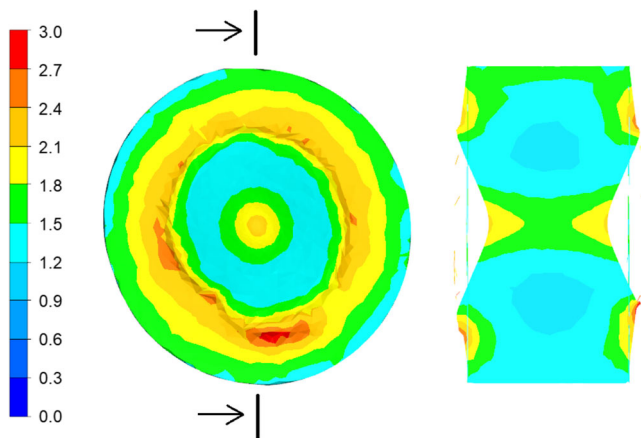Fig. 14 Distribution of stress triaxiality at points 1, 2, and 3 on the specimen's axis, with T = 1000 °C

Fig. 15 Numerically predicted distribution of effective strain in a specimen subjected to rotational compression between channel-dies, with the billet preheated to 1100 °C

that the channel-die rotational compression test had been modelled correctly.

Results and discussion

This section presents the results of experiments aimed at establishing a critical damage value (C_{CL}) for the 50HS grade steel (1.5026).

As previously mentioned, during the experiments, critical forming lengths (*s*) were determined for six billet temperatures. The ranges of the temperatures and forming lengths considered in the tests are given in Fig. 19. The following critical forming lengths (*s*) were established: 150 mm for a billet preheated to $T = 950$ °C, 175 mm for $T = 1000$ °C, 185 mm for $T = 1050$ °C, 275 mm for $T = 1100$ °C, 325 mm for $T = 1150$ °C, and 375 mm for $T = 1200$ °C.

To determine the critical damage values for 50HS steel (1.5026), numerical simulations of critical cases were performed. To precisely monitor the damage function and
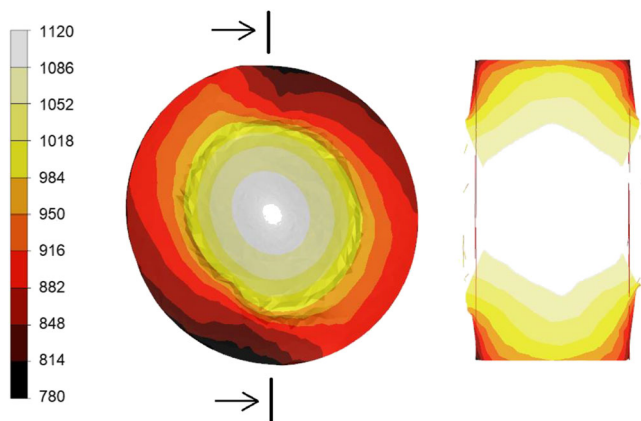

Fig. 16 Numerically predicted distribution of temperature in a specimen subjected to rotational compression between channel-dies, with the billet preheated to 1100 °C
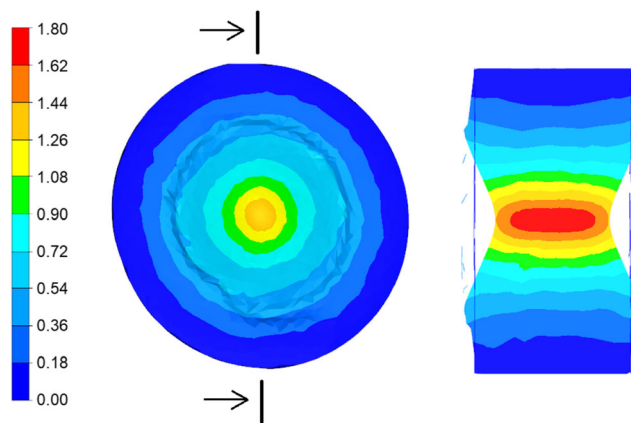

Fig. 17 Numerically predicted distribution of the Cockcroft –Latham damage function in specimen subjected to rotational compression between channel-dies, with the billet preheated to 1100 °C

temperature, 11 virtual sensors were placed along the specimen's axis. They were spaced every 2 mm. The sample temperature and CL damage function distribution curves obtained during compression are shown in Figs. 20 and 21, respectively. The temperature curves show that the material in the centre of the specimen did not cool down at all; on the contrary, the temperature clearly increased, which was undoubtedly the result of plastic work being converted into heat. Even on the specimen's side face (sensors 1 and 11), where a slight cooling of the material was initially noted, the temperature returned to the initial value at the end of the test. An analysis of the data shown in Fig. 21 demonstrates that the damage function grew (almost) steadily throughout the test. The smallest increases for this function are observed for the side faces, where the deformations of the material are larger than those in the centre (Fig. 15). This means that the stress state in the centre of the specimen was more favourable to material cracking than the shear stresses observed on the end faces.
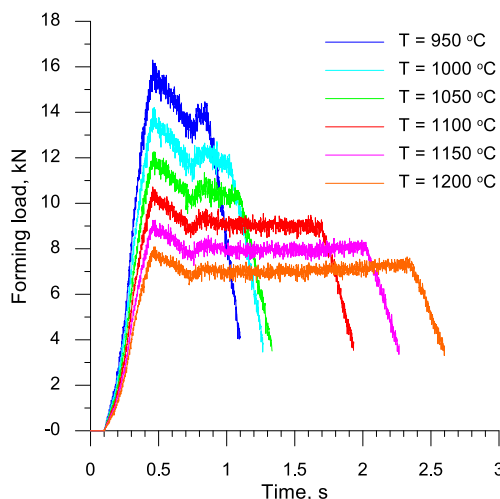

Fig. 18 Numerically calculated distributions of forming loads in tests of rotational compression between channel-dies, as function of billet temperature *T*
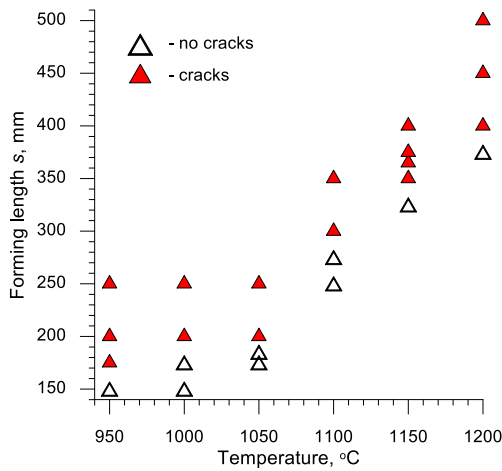
Fig. 19 Temperature and forming length ranges considered in the experiments performed to determine critical material cracking values in a test of rotational compression of 50HS steel (1.5026) specimen between channel-dies

Fig. 21 Changes in the Cockcroft –Latham damage function at points located on the specimen's axis (as shown in the graph) for test performed at 1100 °C with specimen rotated over critical forming length

The final temperature and damage function values recorded using the individual sensors were used to determine the distributions of these parameters along the specimen's axis after the compression tests. The temperature distributions are shown in Fig. 22, and the damage function distributions are presented in Fig. 23. The data given in these figures show that both the temperature and damage function values were the lowest on the outer surface and the highest in the central part of the specimen. It is worth emphasising that the graphs were plotted taking into account changes in the positions of the virtual sensors during rotational compression. Figures 22 and 23 clearly show that the extreme points of the curves (corresponding to the positions of sensors 1 and 11) are shifted along the specimen's axis. The size of this shift, corresponding to the depth of the concavity in the side face of the specimen, increases with forming length s, which is longer with a
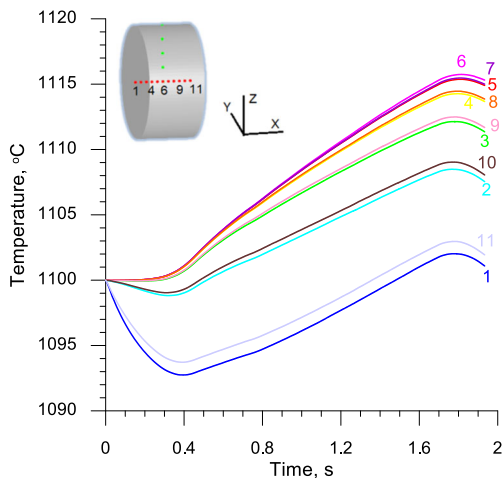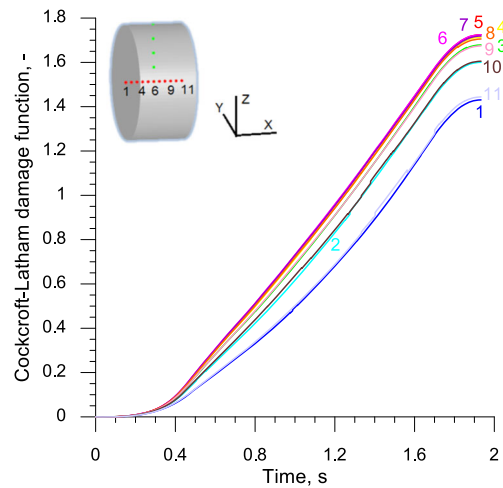
higher initial temperature for the billet. The maximum shift (concavity depth) recorded at 1200 °C was 4 mm and was in good agreement with the depth of the concavity measured in the specimen obtained in the experimental tests.

The final values of the damage function and temperature were used to determine the critical damage values for the tested steel. To this end, the values for the temperature and damage function CL obtained from individual sensors were first averaged. Next, these data are used to generate a graph (Fig. 24), with mean temperatures plotted on the abscissa axis, and mean damage function values plotted on the ordinate axis. The study showed that the temperature had an impact on the critical damage value. An increase in temperature caused an increase in critical damage, which grew quite slowly in the temperature range of 950–1050 °C, but increased much more rapidly at higher temperatures.

For practical applications, the relationship between the critical damage value C_{CL} of 50HS (1.5026) steel and

Fig. 20 Temperature changes at points located on the specimen's axis as shown in the graph for test performed at 1100 °C with specimen rotated over the critical forming length
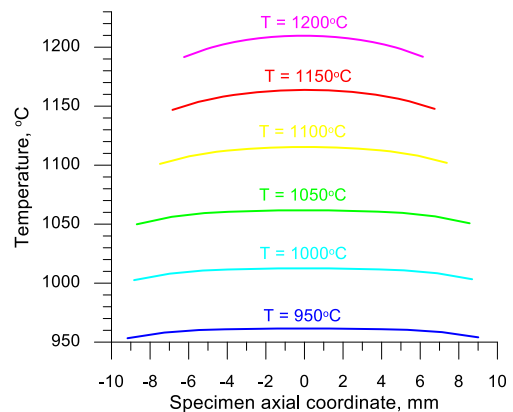

Fig. 22 Distribution of temperature (in °C) along the axis of a specimen subjected to rotational compression (at the critical time, i.e. when the material is predicted to crack)
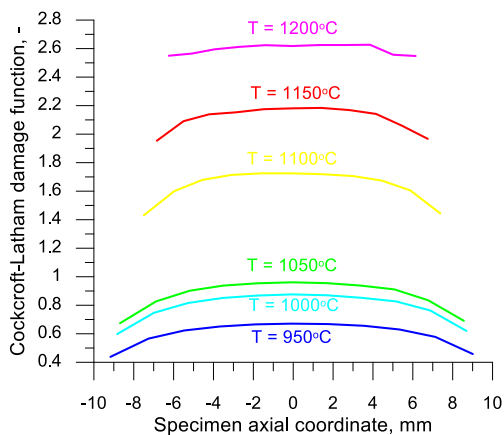
Fig. 23 Distribution of the Cockcroft –Latham damage function along the axis of a specimen subjected to rotational compression (at critical time, i.e. when the material is predicted to crack)

temperature T can be described using the following system of equations:

$$\left.\begin{array}{l} C_{CL} = 0.00274\ T - 2.02 \quad \text{for} \quad 950°C < T \leq 1055°C \\ C_{CL} = 0.01178\ T - 11.54 \quad \text{for} \quad 1055°C < T \leq 1210°C \end{array}\right\} \cdot (4)$$

Conclusions

The results of the study led to the following conclusions:

- In the test of rotational compression between channel-dies, cracking occurred in the axial zone of the specimen.
- As the specimen was rotated, radial stresses along the axis of the specimen changed cyclically from compressive to tensile and back again, which, after the specimen had made a critical number of revolutions, led to the formation of a crack.
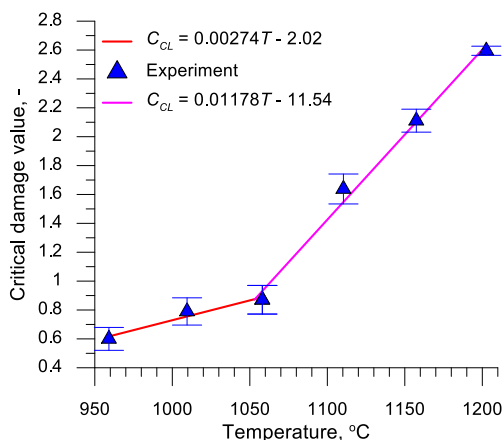

Fig. 24 Relationship between critical fatigue of 50HS steel (1.5026) and temperature established in the test of rotational compression between channel-dies

- Despite the relatively long duration of the test under hot forming conditions, the temperature of the material in the axial zone of the specimen did not decrease, but, on the contrary, increased slightly as a result of the conversion of plastic work into heat.
- To determine the critical value of damage at a given temperature using the rotational compression test, it was necessary to determine the critical forming length at which cracking occurred.
- The critical value of material damage determined in the channel-die rotational compression test depended on the temperature of the test material, with an increase in temperature causing an increase in the critical value of damage.
- Rotational compression in a channel is recommended to determine the critical values of material fatigue used in analyses of cross- and skew-rolling processes. In the case of hot rolling 50HS (1.5026) grade steel, the application of the equations shown in (4) is recommended.

Compliance with ethical standards

References

1. Ceretti E, Giardini C, Attanasio A (2001) Analysis of rotary tube piercing process: simulation and experimental results. In: Proceedings of AITEM 01, September 2001, Bari, Italy
2. Capoferri G, Ceretti E, Giardini C, Attanasio A (2002) FEM analysis of rotary tube piercing process. Tube Pipe Technology, May/June 55–58
3. Ceretti E, Giardini C, Attanasio A, Brisotto F, Capoferri G (2004) Rotary tube piercing study by FEM analysis: 3D simulations and experimental results. Tube & Pipe Technology, March/April 155–159
4. Pater Z, Kazanecki J, Bartnicki J (2006) Three dimensional thermo-mechanical simulation of the tube forming process in Diescher's mill. J Mater Process Technol 177:167–170. https://doi.org/10.1016/j.jmatprotec.2006.03.205
5. Fanini S, Bruschi S, Ghiotti A (2008) Modelling of Mannesmann fracture initiation during cross-roll piercing. In: Proceedings of the 12th metal forming international conference, Krakow, Poland, 357–363

6. Chastel Y, Diop A, Fanini S, Bouchard PO, Mocelin K (2008) Finite element Modelling of tube piercing and creation of a crack. Int J Mater Form Suppl 1:355–358. https://doi.org/10.1007/s12289-008-0068-2

7. Ghiotti A, Fanini S, Bruschi S, Bariani PF (2009) Modelling of the Mannesmann effect. CIRP Ann– Manuf Technol 58:255–258. https://doi.org/10.1016/j.cirp.2009.03.099

8. Pater Z, Tofil A (2014) FEM simulation of the tube rolling process in Diescher's mill. Adv Sci Technol Res J 8(22):51–55. https://doi.org/10.12913/22998624.1105165

9. Skripalenko MM, Romantsev BA, Galkin SP, Skripalenko MN, Kaputkina LM, Tran Ba H (2018) Prediction of the fracture of metal in the process of screw rolling in a two-roll mill. Metallurgist 61(11–12):925–933. https://doi.org/10.1007/s11015-018-0588-z

10. Yang H, Zhang L, Hu Z (2012) The analysis of the stress and strain in skew rolling. Adv Mater Res 538–541:1650–1653. https://doi.org/10.4028/www.scientific.net/AMR.538-541.1650

11. Pater Z, Tomczak J, Bartnicki J, Lovell MR, Menezes PL (2013) Experimental and numerical analysis of helical-wedge rolling process for producing steel balls. Int J Mach Tool Manu 67:1–7. https://doi.org/10.1016/j.ijmachtools.2012.12.006

12. Cao Q, Hua L, Qian D (2015) Finite element analysis of deformation characteristics in cold helical rolling of bearing steel-balls. J Cent South Univ 22(4):1175–1183. https://doi.org/10.1007/s11771-015-2631-6

13. Pater Z (2016) Numerical analysis of helical rolling processes for producing steel balls. Int J Mater Prod Technol 53(2):137–153. https://doi.org/10.1504/IJMPT.2016.076417

14. Pater Z, Tomczak J (2018) FEM modelling of a helical wedge rolling process for axisymmetric parts. Adv Sci Technol Res J 12(1):115–126. https://doi.org/10.12913/22998624/81767

15. Pater Z, Tomczak J, Bartnicki J, Bulzak T (2018) Thermomechanical analysis of a helical-wedge rolling process for producing balls. Metals-Basel 8(11):862. https://doi.org/10.3390/met8110862

16. Tomczak J, Pater Z, Bulzak T (2018) The effect of process parameters in helical rolling of balls on the quality of products and the forming process. Materials 11(11):2125. https://doi.org/10.3390/ma11112125

17. Pater Z, Tomczak J, Bulzak T, Martyniuk S (2019) A helical wedge rolling process for producing a ball pin. Proc Manuf 27:27–32. https://doi.org/10.1016/j.promfg.2018.12.039

18. Murillo-Marrodan A, Garcia E, Cortes F (2018) A study of friction model performance in a skew rolling process numerical simulation. Int J Simul Model 17(4):569–582. https://doi.org/10.2507/IJSIMM17(4)441

19. Li H, Fu MW, Lu J, Yang H (2011) Ductile fracture: experiments and computations. Int J Plasticity 27:147–180. https://doi.org/10.1016/j.ijplas.2010.04.001

20. McClintock FA (1968) A criterion of ductile fracture by growth of holes. J Appl Mech 35:363–371. https://doi.org/10.1115/1.3601204

21. Rice JR, Tracey DM (1969) On the ductile enlargement of voids in triaxial stress fields. J Mech Phys Solids 17:201–217. https://doi.org/10.1016/0022-5096(69)90033-7

22. Cockcroft MG, Latham DJ (1968) Ductility and the workability of metals. J I Met 96:33–39

23. Sebek F (2016) Ductile fracture criteria in multiaxial loading – theory, experiments and application. Doctoral Thesis. Brno University of Technology, Czech Republic